Coordinated Supplementary Damping Control of DFIG and PSS to Suppress Inter-Area Oscillations with Optimally Controlled Plant Dynamics

Chen Zhang, *Student Member, IEEE*, Deping Ke, Yuanzhang Sun, *Senior Member, IEEE*, C. Y. Chung, *Fellow, IEEE*, Jian Xu, *Member, IEEE*, Feifan Shen

***Abstract*—This paper proposes a design method to coordinate dual-channel supplementary damping controllers (SDCs) of doubly-fed induction generators (DFIGs) and power system stabilizers (PSSs) for suppression of inter-area power oscillations. A dynamic performance index is introduced to measure the dynamics of the conventional synchronous generator (SG) and DFIG during the damping control process. Hence, the proposed method designing the PSS and SDC is formulated as an optimization problem with the objective function being the sum of weighted performance indexes and the constraints indicating the requirements on the damping of the inter-area modes. Solving the optimization problem can obtain the optimal SDC and PSS which can meet the required damping results as well as optimize dynamics of the controlled plants. Moreover, by adjusting weights in the objective function, the damping control burden can be flexibly and feasibly allocated between active and reactive power channels of DFIGs or among the damping controllers. Simulations with the modified New England and New York interconnected system prove that the proposed optimization based tuning method can not only robustly coordinate the PSS and SDC to effectively damp inter-area oscillations but also improve the dynamics of controlled plants during the damping control process over different operating conditions.**

***Index Terms*—Doubly-fed induction generator, inter-area oscillation damping, dynamic performance, coordination control, active and reactive power modulation.**

I. Introduction

WITH increased penetration of wind power in large-scale power systems, new challenges inevitably arise with respect to stable and reliable system operations [1], [2]. Doubly-fed induction generators (DFIGs) have been widely used for wind power harnessing because they have excellent control flexibility and can accommodate grid code requirements. Because large wind farms are usually located in remote areas and weakly connected to power grids by long-distance transmission lines, inter-area power oscillations among synchronous generators (SGs) can also adversely affect the wind power generation. Additionally, grid-connected DFIGs would displace some SGs to maintain power balance, which therefore changes the power flow of the system. Consequently, the problem of inter-area oscillations problem can become more complicated due to grid-connected DFIGs. In particular, some literatures report that power oscillations of inter-area modes might further deteriorate due to installation of large-scale DFIGs [3]-[6]. Therefore, studies on driving DFIGs to contribute to the damping control of electromechanical power oscillations have received much more attentions in recent years [4]-[15].

A supplementary damping controller (SDC) that manipulates the rotor side converter (RSC) to modulate DFIG's power outputs, has proven to be as an effective auxiliary means to suppress inter-area oscillations in power systems [7]. Stator-voltage-oriented vector control is generally applied to regulate the active and reactive power outputs of a DFIG so that they can be effectively decoupled [8]. Correspondingly, the damping control via supplementary power modulation can be divided into active power modulation (PM) and reactive power modulation (QM). References [9]-[14] commonly add the auxiliary damping signal produced by the SDC to the control reference of active power, which modulates the active power output of the DFIG so as to damp inter-area oscillations. In contrast, in [15]-[19] the damping signal is added to the reactive power control reference so that the DFIG's reactive power output is modulated. Moreover, it should be pointed out that although PM is more effective than QM by directly changing the electromagnetic torque of generators, PM has the risk of deteriorating the shaft dynamics of the DFIG while QM is immune to such adverse interactions. However, QM can quite possibly worsen the stator voltage dynamics [19]. Hence, the problem is that the DFIG has to partially sacrifice itself dynamics to engage in the damping control, which indicates the need for a trade-off by the DFIG between the damping control and its dynamic performance. Namely, these previous studies primarily focus on the damping effects of power oscillations by modulating DFIGs but rarely care about DFIGs' dynamics.

Coordination of power system stabilizer (PSS) and SDC installed to the DFIG is effective to mitigate inter-area oscillations in power systems integrated with large-scale DFIG-based wind generation. By using the optimal partial eigenstructure assignment method, the active damping controller for a DFIG (by PM) in [20] is devised in cooperation with the PSS. Reference [21] proposes a coordinated robust control strategy to tune the damping controller of a DFIG (by QM) and the PSS considering system uncertainties. Furthermore, a tuning method based on the placement of probabilistic eigenvalues is pro-

This work was supported by the National Natural Science Foundation of China under Grant 51777143.

C. Zhang, D. Ke (corresponding author), Y. Sun, J. Xu and F. Shen are with the School of Electrical Engineering, Wuhan University, Wuhan 430072, China (e-mail: eezhangchen@whu.edu.cn; kedeping@whu.edu.cn).

C. Y. Chung is with the Department of Electrical and Computer Engineering, University of Saskatchewan, Saskatoon, SK S7N 5A9, Canada (e-mail: c.y.chung@usask.ca).

posed in [22] to coordinate the SDC (installed in the QM channel) and the PSS. However, the main pursuit of these coordination methods is the maximum damping effects for the inter-area oscillations but they can hardly deal with the issues like how to reasonably and flexibly assign the damping control burden between the PSS and SDC. Apparently, the unexpected consequence could be excessive damping effects or intolerant dynamics of controlled plants during the damping control process.

In order to address aforementioned two issues, this paper proposes a design method to coordinately tune the SDC of DFIG and the PSS for damping inter-area oscillations with the optimal dynamics of controlled plants. The contributions of this paper are summarized, as follows:

1) In addition to supplying the desired damping results to the inter-area oscillations, the proposed design method can also optimize the dynamics of the SG and DFIG (e.g., the terminal voltage dynamics of the SG), and relieve excessive adverse impacts (e.g., deterioration on the shaft torsional dynamics of the DFIG) caused by the engagement of DFIGs in the damping control.
2) Based on a dual-channel SDC to simultaneously modulate active and reactive power outputs of the DFIG, the proposed design method can flexibly and feasibly allocate the damping control burden between the two channels of the DFIG. Similarly, the damping control burden can also be assigned among various damping controllers, such as the SDC and PSS.

The remainder of this paper is organized as follows. General models of the DFIG-based wind turbine generator (WTG) and the dual-channel SDC are introduced in Section II. Section III and IV introduce the employed dynamic performance index and the proposed optimization method to tune parameters of damping controllers. Simulations and discussion of the test system are conducted in Section V. Finally, Section VI concludes the paper.

II. Modeling DFIG-based WTG

A DFIG-based WTG is a complicated piece of equipment that couples mechanics, electrics, and magnetics. However, the electromechanical dynamics are the main concerns in this paper which are used to investigate the response of the WTG in the time scale of power oscillations. Thus, models of the WTG's components (Fig. 1) which can adequately capture the electromechanical dynamics are described in the following.

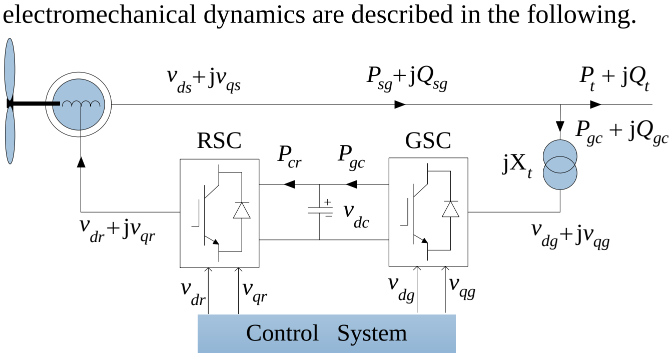

Fig. 1. Detailed structure of a DFIG-based WTG.

A. Wind Turbine and DFIG Model

In this paper, the wind turbine together with the DFIG rotating mass is represented by a two-mass model to take into account the torsional mode associated with the shaft. Additionally, for electromechanical transient simulations, fast stator dynamics of the induction generator are normally neglected to ensure compatibility with the other system component models, particularly the transmission network, as shown in Fig. 1. Therefore, the model of wind turbine and DFIG can be represented as follows:

$$\frac{d\theta_{tw}}{dt} = \omega_b(\omega_t - \omega_r) \tag{1}$$

$$\frac{d\omega_t}{dt} = \frac{1}{2H_t}\left[T_m - K_{tw}\theta_{tw} - D_{tw}(\omega_t - \omega_r)\right] \tag{2}$$

$$\frac{d\omega_r}{dt} = \frac{1}{2H_g}\left[K_{tw}\theta_{tw} + D_{tw}(\omega_t - \omega_r) - T_e\right] \tag{3}$$

$$\frac{1}{\omega_b}\frac{de_d}{dt} = -\frac{1}{T_0}[e_d - (X - X')i_{qs}] + s\omega_s e_q - \omega_s\frac{L_m}{L_m + L_r}v_{qr} \tag{4}$$

$$\frac{1}{\omega_b}\frac{de_q}{dt} = -\frac{1}{T_0}[e_q + (X - X')i_{ds}] - s\omega_s e_d + \omega_s\frac{L_m}{L_m + L_r}v_{dr} \tag{5}$$

where θ_{tw} is the shaft twist angle; ω_t and ω_r are the angular speeds of the turbine and the DFIG rotor, respectively; ω_b is the system speed base in the units of rad/s; K_{tw} and D_{tw} are coefficients to denote the shaft stiffness and mechanical damping effect, respectively; H_t and H_g are inertia time constants of the wind turbine and the DFIG, respectively; e is the internally generated voltage, v_r is the rotor voltage, i_s is the stator current, 'd' or 'q' subscripts for these variables indicating d-axis or q-axis components, respectively; ω_s is the synchronous speed; s is the slip; L_m and L_r are the magnetizing inductance and rotor inductance, respectively; T_0 is the transient open-circuit time constant; X and X' are the open-circuit and short-circuit reactance, respectively; T_e is the electromagnetic torque. Especially, T_m is the mechanical torque of the wind turbine, which is calculated using:

$$T_m = \frac{P_m}{\omega_r} = \frac{0.5\rho\pi R^2 C_p(\lambda,\beta)V_w^3}{\omega_r} \tag{6}$$

where P_m is the mechanical power; ρ is the air density; R is the wind turbine radius; V_w is the wind speed; and C_p is the power coefficient which is a function of the pitch angle β and the tip speed ratio λ, defined as:

$$\lambda = \frac{\omega_r R}{V_w} \tag{7}$$

It is noted in (6) and (7) that P_m is a variable because C_p changes as ω_r fluctuates with power oscillations. This is different from SGs, the mechanical power of which is usually observed to be constant during electromechanical transients.

B. Primary Controllers of DFIG Converts

According to the principle of stator-voltage-oriented vector control, managing the active and reactive power output of the DFIG is accomplished by controlling the RSC. The block diagrams of the primary controllers of the RSC are shown in Fig.

2. The q-axis control loop, which generates the control signal v_{qr}, is used to regulate the active power output of the DFIG. In particular, the power reference P_{opm} is obtained through a simplified maximum power point tracking (MPPT) algorithm. For a fixed pitch angle β, the optimal power coefficient C_{pmax} can be calculated based on the analytical function of $C_p(\lambda,\beta)$. Apparently, since the pitch angle is fixed, C_{pmax} will remain unchanged so that the maximum P_m can be computed from (6) with the measurement of wind speed [23]. In this paper, the DFIG outputs the constant reactive power in the steady state by the d-axis control loop, which produces the control signal v_{dr}.

The control objectives of the grid side convert (GSC) are to maintain the DC link voltage as well as drive the GSC reactive power output to follow the reference. Thus, the primary controllers of the GSC are depicted in Fig. 3.

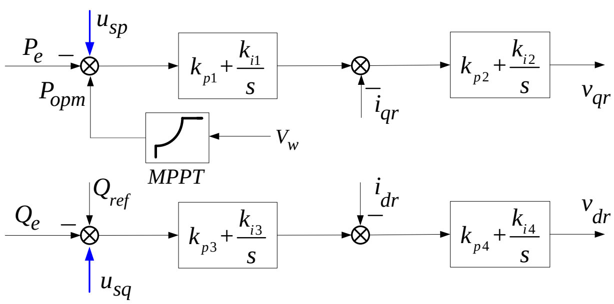

Fig. 2. Block diagram of RSC primary controllers.

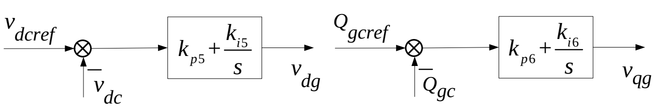

Fig. 3. Block diagram of GSC primary controllers.

C. Supplementary Dual-Channel Damping Control

Because the active and reactive power control loops are well decoupled by the vector control scheme, it was observed in [19] that an SDC attached to the active power control loop of the DFIG mainly impacts its active power output while an SDC installed in the reactive power control loop principally influences the reactive power output. As mentioned previously, PM and QM for damping control have fairly different impacts on DFIG dynamics. So, in order to give more flexibility for the DFIG to participate in the damping control as well as to optimize DFIG dynamics, a dual-channel SDC (Fig. 4) is proposed in this paper to modulate active and reactive power outputs of the DFIG simultaneously by generating supplementary signals (u_{sp} and u_{sq}) to the two primary control loops in Fig. 2.

Compared to the structure of SDCs in [24], the PM and QM channels in the proposed SDC commonly employ the conventional PSS structure: each channel is composed of a gain block and two phase lead-lag compensation blocks. Apparently, the proposed SDC is a structurally-constrained controller since only certain parameters (e.g. K_p, T_{p1}) can be tuned. Additionally, the washout and dead-band blocks are shared by two channels so that the SDC is ineffective in the steady state and also not engaged by the ambient noisy signals. Moreover, limiters can properly constrain the SDC's outputs u_{sp} and u_{sq} to prevent excessive control effort from the DFIG.

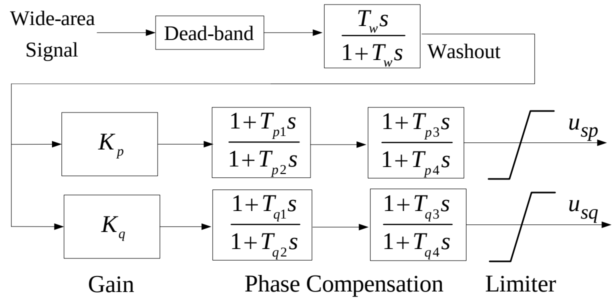

Fig. 4. Block diagram of the proposed dual-channel SDC.

III. Introduction of Dynamic Performance Index

A. Preparation to Design Wide-Area Controllers

Two preparations must be done before formulating the closed-loop power system to design wide-area damping controllers PSSs and SDCs:

1) A reduced-order model of the open-loop power system is computed. Usually, the models of a real large-scale power system have fairly high dimension, up to tens of thousands. For electromechanic oscillation simulations, however, the dynamics of interest mainly cover a frequency range from 0.1 to 2 Hz. Therefore, a reduced-order model of the open-loop power system can be obtained to well approximate the original high-order model. In this paper, the Schur method [25] is applied for balanced model truncation of the simulated power system.

2) In general, the time delays existing in the feedback channels of wide-area signals are considerable, and could bring unexpected impacts on control effects if they are overlooked during the control design. Therefore, tuning of the damping controllers in this paper takes into account the time delay and approximates it using the following Pade formula [26]:

$$e^{-\tau s} \approx \frac{\tau^2 s^2 - 6\tau s + 12}{\tau^2 s^2 + 6\tau s + 12} \tag{8}$$

where $\boldsymbol{\tau}$ is the time delay.

B. A Brief Description of the Dynamic Performance Index

The linearized model of a closed-loop power system with damping controllers in the jth operating condition can be generally described, as follows:

$$\dot{\boldsymbol{x}}_j = \boldsymbol{A}_j\,\boldsymbol{x}_j \qquad \boldsymbol{y}_o = \boldsymbol{E}_j\,\boldsymbol{x}_j \qquad \boldsymbol{u}_c = \boldsymbol{K}_j\,\boldsymbol{x}_j \tag{9}$$

where $\boldsymbol{x}_j \in \Re^n$ is the state vector that consists of increments of the state variables (e.g., power angles, angular speeds, etc.) with respect to their steady-state values; $\boldsymbol{A}_j$ is the state matrix; $\boldsymbol{y}_o$ is the vector comprising observed variables that are specially chosen for the control objectives; $\boldsymbol{u}_c$ is the output vector of the damping controllers; and $\boldsymbol{E}_j$ and $\boldsymbol{K}_j$ are the matrices indicating linear mapping from the states to $\boldsymbol{y}_o$ and $\boldsymbol{u}_c$, respectively. The details of deducing (9) are given in Appendix A. It should be noted that some variables with bold face indicate matrices or vectors in this paper.

For the dynamic analysis of power systems, the state matrix $\boldsymbol{A}_j$ can be similarly diagonalized. Thus, the time domain solution $\boldsymbol{x}_j(t)$ of (9) can be derived as follows:

$$\boldsymbol{x}_j(t)=\boldsymbol{U}_j\boldsymbol{e}^{\boldsymbol{\Lambda}_j t}\boldsymbol{V}_j\boldsymbol{x}_{j0} \qquad t>0 \tag{10}$$

where $\boldsymbol{U}_j$ and $\boldsymbol{V}_j$ are the right and left eigenvector matrices of $\boldsymbol{A}_j$, respectively; $\boldsymbol{x}_{j0}$ denotes the initial value of the state vector; and $\boldsymbol{\Lambda}_j$ is a diagonal matrix comprised of eigenvalues ($\lambda_{j1}, \lambda_{j2},\ldots, \lambda_{jn}$) of $\boldsymbol{A}_j$, defined as follows:

$$\boldsymbol{\Lambda}_j = diag\left(\lambda_{j1}, \lambda_{j2}, ..., \lambda_{jn}\right) \tag{11}$$

A quadratic index (cost function) measuring the dynamic performance of the system is defined as follows:

$$cost_j = \int_0^\infty \boldsymbol{y}_o^{\boldsymbol{H}} \boldsymbol{Q}\, \boldsymbol{y}_o\, dt \qquad \boldsymbol{x}_j(0) = \boldsymbol{x}_{j0} \tag{12}$$

where $\boldsymbol{Q}$ is a diagonal weight matrix. The cost function (12) is positive for any given $\boldsymbol{x}_{j0}$. However, $\boldsymbol{x}_{j0}$ is usually undetermined (and associated with disturbances) for real power systems so that the cost function is difficult to use directly to optimize the parameters of damping controllers.

If the system is stable and all eigenvalues of $\boldsymbol{A}_j$ have with negative real parts, then (11) can be calculated as follows:

$$cost_j = \int_0^\infty (\boldsymbol{E}_j\boldsymbol{x}_j)^{\boldsymbol{H}} \boldsymbol{Q}\, (\boldsymbol{E}_j\boldsymbol{x}_j)\, dt = \boldsymbol{x}_{j0}^{\boldsymbol{H}}\boldsymbol{M}_j\boldsymbol{x}_{j0} \tag{13}$$

where $\boldsymbol{M}_j$ is termed the cost matrix and is a positive definite matrix defined as:

$$\boldsymbol{M}_j = \boldsymbol{V}_j^{\boldsymbol{H}}\left[\left(\boldsymbol{U}_j^{\boldsymbol{H}}\boldsymbol{E}_j^{\boldsymbol{H}}\boldsymbol{Q}\,\boldsymbol{E}_j\boldsymbol{U}_j\right)\cdot\boldsymbol{L}_j\right]\boldsymbol{V}_j \tag{14}$$

where ‘ · ’ is the dot-product operator; and $\boldsymbol{L}_j$ is a Hermite matrix whose entry in the position of the kth row, lth column is defined as:

$$\boldsymbol{L}_j(k,l) = -\frac{1}{\lambda_{jk}^* + \lambda_{jl}} \tag{15}$$

where $*$ is the conjugate operator.

Nevertheless, because $\boldsymbol{M}_j$ is a positive definite Hermite matrix, the singular values matrix of $\boldsymbol{M}_j$ could be regarded as a scaling matrix in geometrical transformations. This means that singular values of $\boldsymbol{M}_j$ could depict the intrinsic characteristics of the closed-loop system and have no relationship with $\boldsymbol{x}_{j0}$. Moreover, reducing them has the same effect as decreasing (12) and (13). Hence, the index to gauge the dynamic performance of the system can be constructed as follows:

$$f_j = \sum_{k=1}^{n}\sigma_{jk} \tag{16}$$

where $\sigma_{j1},\sigma_{j2},...,\sigma_{jn}$ are the singular values of $\boldsymbol{M}_j$ and the sum of these is defined in this paper as the performance index.

C. Dynamic Performance Index Construction for Coordinated Damping Control by SG and DFIG

Some pioneer studies have proposed various tuning methods for damping controllers to mitigate inter-area oscillations; they actually tune the damping controllers by minimizing (or maximizing) quite different objective functions, such as power angle differences [27] or damping ratios of inter-area modes [19]-[22]. These methods can obtain fairly satisfactory damping control effects but hardly care about the dynamics of controlled plants. Nevertheless, it has been addressed in [28] that the terminal voltage of SGs will be sacrificed (deteriorated) as they are driven (by PSSs) to suppress electromechanical oscillations. Besides, DFIGs’ dynamics will also be comparatively degraded by supplementarily installed SDCs during the damping control process [19]. Hence, by reasonably selecting observed variables $\boldsymbol{y}_o$, the new performance index (16) introduced in this paper can quantitatively measure the dynamics of controlled plants (e.g. SGs and DFIGs). It can be inferred that the damping controllers which maximize/minimize the specifically devised dynamic performance indices can not only accomplish the damping control task but also optimize the controlled plants’ dynamics.

As for observed variables $\boldsymbol{y}_o$ in (9), the terminal voltage V_g of SGs is picked out as the dynamic performance measurement. Additionally, observed variables selected for the DFIG are its active and reactive power outputs (P_g and Q_g) as they are dual-channel modulated. Hence, according to (8), these observed variables can be expressed as follows:

$$V_g = \boldsymbol{E}_v\boldsymbol{x} \qquad P_g = \boldsymbol{E}_p\boldsymbol{x} \qquad Q_g = \boldsymbol{E}_q\boldsymbol{x} \tag{17}$$

where $\boldsymbol{E}_v$, $\boldsymbol{E}_p$ and $\boldsymbol{E}_q$ have the same meaning as that of $\boldsymbol{E}$ in (9). Accordingly, the following cost functions can be constructed:

$$cost_v = \int_0^\infty V_g^2\, dt \quad cost_p = \int_0^\infty P_g^2\, dt \quad cost_q = \int_0^\infty Q_g^2\, dt \tag{18}$$

Furthermore, the corresponding indices depending on (16) can be calculated:

$$f_v = \sum_{k=1}^{n}\sigma_{vk} \qquad f_p = \sum_{k=1}^{n}\sigma_{pk} \qquad f_q = \sum_{k=1}^{n}\sigma_{qk} \tag{19}$$

These indices can be used as objective functions to tune the parameters of the PSSs and dual-channel SDCs so that the dynamics of the SGs and DFIGs can be optimized as they are engaged in the damping control of inter-area oscillations.

IV. Optimal Tuning of Damping Controllers

A. Formulation of Optimization Problem

Together with the models of PSSs and SDCs (introduced in Subsection II-C), the closed-loop model (9) can be synthesized to formulate the optimization problem which is used for the control design. In particular, the state matrix $\boldsymbol{A}_j$ of the closed-loop power system is constructed by using the models of the time delays, the damping controllers and the reduced-order open-loop power system, as follows (Appendix A):

$$\boldsymbol{A}_j = \begin{bmatrix} \boldsymbol{A}_{jr} + \boldsymbol{B}_{jr}\boldsymbol{D}_c\boldsymbol{D}_\tau\boldsymbol{C}_{jr} & \boldsymbol{B}_{jr}\boldsymbol{D}_c\boldsymbol{C}_\tau & \boldsymbol{B}_{jr}\boldsymbol{C}_c \\ \boldsymbol{B}_\tau\boldsymbol{C}_{jr} & \boldsymbol{A}_\tau & \boldsymbol{0} \\ \boldsymbol{B}_c\boldsymbol{D}_\tau\boldsymbol{C}_{jr} & \boldsymbol{B}_c\boldsymbol{C}_\tau & \boldsymbol{A}_c \end{bmatrix} \tag{20}$$

Moreover, to ensure the robustness of the damping controllers (PSSs and SDCs), multiple operating conditions (including the ones with outages of important tie-lines) are considered during the design process. Based on the index (19), optimal coordination of the PSSs and SDCs to suppress inter-area oscillations can be converted into an optimization problem that searches optimal parameters of the PSSs and SDCs, as follows:

$$\min_{\boldsymbol{P}} \quad \sum_{j=1}^{N_o}\omega_j\left(\sum_{k=1}^{N_v}\omega_{kv} f_{j.kv}+\sum_{l=1}^{N_w}\omega_{lp} f_{j.lp}+\sum_{l=1}^{N_w}\omega_{lq} f_{j.lq}\right) \tag{21a}$$

$$s.t. \qquad \xi_{a\min} \le \xi_{ja} \le \xi_{a\max} \qquad \lambda_{ja} \in \pi_{c1} \tag{21b}$$

$$\omega_{a\min} \le \omega_{ja} \le \omega_{a\max} \tag{21c}$$

$$\xi_{jb} \le \xi_{b\,c} \qquad \lambda_{jb} \in \pi_{c2} \tag{21d}$$

$$\alpha_{jb} \le \alpha_{b\,c} \qquad j=1,\ldots N \tag{21e}$$

$$\boldsymbol{P}_{\mathbf{min}} \le \boldsymbol{P} \le \boldsymbol{P}_{\mathbf{max}} \tag{21f}$$

where N_o is the number of the considered operating conditions and ω_j is the weight of the jth operating condition; N_v and N_w are the numbers of PSSs and SDCs, respectively; ω_{kv}, ω_{lp}, and ω_{lq} are the weights of the indices $f_{j.kv}$, $f_{j.lp}$ and $f_{j.lq}$, respectively; $\boldsymbol{P}$ with the following definition (21) is the adjustable parameters vector of the damping controllers (PSSs and SDCs), and $\boldsymbol{P}_{\mathbf{min}}$ and $\boldsymbol{P}_{\mathbf{max}}$ are the lower and upper limits of $\boldsymbol{P}$, respectively.

$$\boldsymbol{P}=\left[K_1,T_{11},T_{12},T_{13},T_{14},\ldots,K_n,T_{n1},T_{n2},T_{n3},T_{n4}\right]^{\boldsymbol{H}} \tag{22}$$

where n is the total number of damping controllers, including PSSs and SDCs.

B. Discussion

The objective function (21a) of the optimization model is a measurement of the dynamic performance of the SGs and DFIGs during the damping control process. Apparently, smaller ω_v will lead to the PSSs playing dominant roles in the damping control, which means that the terminal voltage dynamics of the SGs will be considerably deteriorated. Similarly, smaller ω_p indicates that the DFIGs will more intensively exert their active power capacities to damp inter-area oscillations, which tends to bring more adverse impacts on the dynamics associated with the active power output of DFIGs, such as the torsional oscillation of shaft. Correspondingly, QM will be more dominant if ω_q is comparatively smaller and hence the dynamics related to the reactive power output of DFIGs will be more obviously worsened. Thus, by adjusting the weights in the objective function, the total damping control burden can be flexibly and feasibly assigned among the PSSs and SDCs so that the dynamics of controlled plants can be optimized.

The constraints (21b)-(21e) proposed in this paper are illustrated in Fig. 5. The concerned modes in this paper would be divided into two types due to their frequency differences between them: the π_{c1} is the set of weakly damped inter-area modes λ_a of the closed-loop power system; π_{c2} is the set consisting of critical modes λ_b that might be deteriorated after the optimization, such as the shaft mode of DFIGs and some local oscillation modes. Moreover, the corresponding constraints for the two types of modes would be also different in the proposed optimization model: ξ_a is the damping ratio of λ_a; $\xi_{a\min}$ and $\xi_{a\max}$ are the lower and upper limits of ξ_a so that inter-area modes could be shifted left to a desirable area after optimization; ω_a is the imaginary part of λ_a; $\omega_{a\min}$ and $\omega_{a\max}$ are the lower and upper limits of ω_a in order to avoid obvious frequency drifts that may cause adverse impacts on the synchronizing torques of generators; ξ_b and α_b are the damping ratio and real part of λ_b; and ξ_{bc} and α_{bc} are the critical values of ξ_b and α_b, respectively, which are set to ensure that the modes in π_{c2} are only slightly influenced after the optimization. Overall, the purpose of the different constraints is to ensure the desired damping ratios of inter-area oscillation modes as well as prevent adversely affecting some of the modes, manifested by deteriorated dynamics of controlled plants.

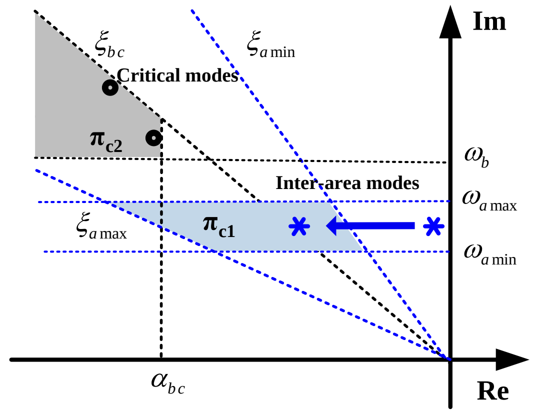

Fig. 5. Illustration of constraints in the proposed optimization model.

As per the discussion above, optimizing the nonlinear problem (21) is an efficient way to achieve optimal damping controller. Consequently, the inter-area modes are properly damped due to application of (21b)-(21c) and the dynamics of the SGs and DFIGs are also improved with objective function (21a) and constraints (21d)-(21e). Therefore, the optimization method proposed in this paper considers controlled plant dynamics and advances other methods in [20], [21], [24], and [29].

C. Solving Optimization Problem

Apparently, the optimization problem (21) is a standard constrained nonlinear programming (NLP) problem. As an effective and mature method for NLP, sequential quadratic programming (SQP) is applied to solve (21) in this paper [30]. In order to conveniently depict the solving process, the optimization model (21) can be expressed in a more general and compact form, as follows:

$$\min_{\boldsymbol{P}} \quad \boldsymbol{F}(\boldsymbol{P}) \tag{23a}$$

$$s.t. \quad \boldsymbol{G}(\boldsymbol{P}) \le 0 \tag{23b}$$

Moreover, the inequality constraints (23b) can be relaxed by establishing the Lagrangian function, as follows:

$$\boldsymbol{L}\left(\boldsymbol{P},\lambda_{\boldsymbol{G}}\right)=\boldsymbol{F}(\boldsymbol{P})+\lambda_{\boldsymbol{G}}\boldsymbol{G}(\boldsymbol{P}) \tag{24}$$

where $\boldsymbol{\lambda_G}$ is the Lagrange multiplier vector for the inequality constraints $\boldsymbol{G}(\boldsymbol{P})$. Then, the following steps are executed [30]:

***Step* 1)** As for the start point, the controller parameters vector $\boldsymbol{P}_1$ are given by the residue method [29], and the positive definite Hessian matrix $\boldsymbol{H}_1$ are initially available and will be updated in the subsequent iteration.

***Step* 2)** Formulate and solve the following convex quadratic programming (QP) subproblem in order to obtain the optimal search direction vector $\boldsymbol{d}_k$ at the kth iteration:

$$\begin{aligned} \min_{\boldsymbol{d}_k} \quad & 0.5\boldsymbol{d}_k^{\boldsymbol{T}}\boldsymbol{H}_k\boldsymbol{d}_k+\nabla\boldsymbol{F}(\boldsymbol{P}_k)^{\boldsymbol{T}}\boldsymbol{d}_k \\ s.t. \quad & \boldsymbol{G}(\boldsymbol{P}_k)+\nabla\boldsymbol{G}(\boldsymbol{P}_k)^{\boldsymbol{T}}\boldsymbol{d}_k \le 0 \end{aligned} \tag{25}$$

where ∇ and T are the hamiltonian and transpose operators, respectively;

***Step* 3)** Execute a linear search method to find the optimal step length $\boldsymbol{\alpha}_k$ along the optimal search direction $\boldsymbol{d}_k$ by minimizing the metric function given by (26). Hence, the controller parameters vector $\boldsymbol{P}_{k+1}$ at the next iteration can be calculated, as follows:

$$\min_{\boldsymbol{\alpha}_k} \quad \left\{ \boldsymbol{F}(\boldsymbol{P}_{k+1}) + \boldsymbol{\rho} \max\left\{ \boldsymbol{0}, \boldsymbol{G}(\boldsymbol{P}_{k+1}) \right\} \right\} \tag{26}$$

$$\boldsymbol{P}_{k+1} = \boldsymbol{P}_k + \boldsymbol{\alpha}_k \boldsymbol{d}_k \tag{27}$$

where $\boldsymbol{\rho}$ is the penalty parameter vector.

***Step* 4)** Check whether the stopping criteria are satisfied. If so, terminate the iterating process; otherwise, go to next step.

***Step* 5)** Update the Hessian matrix $\boldsymbol{H}_{k+1}$ by using the quasi-Newton method, as follows:

$$\boldsymbol{H}_{k+1} = \boldsymbol{H}_k + \frac{\boldsymbol{y}_k \boldsymbol{y}_k^T}{\boldsymbol{y}_k^T \boldsymbol{s}_k} - \frac{\boldsymbol{H}_k \boldsymbol{s}_k \boldsymbol{s}_k^T \boldsymbol{H}_k}{\boldsymbol{s}_k^T \boldsymbol{H}_k \boldsymbol{s}_k} \tag{28a}$$

$$\boldsymbol{s}_k = \boldsymbol{P}_{k+1} - \boldsymbol{P}_k \tag{28b}$$

$$\boldsymbol{y}_k = \boldsymbol{\theta}_k \boldsymbol{J}_k + \left(\boldsymbol{I} - \boldsymbol{\theta}_k \right) \boldsymbol{H}_k \boldsymbol{s}_k \tag{28c}$$

$$\boldsymbol{J}_k = \nabla_{\boldsymbol{P}} \boldsymbol{L}\left(\boldsymbol{P}_{k+1}, \boldsymbol{\lambda}_{\boldsymbol{G}.k+1} \right) - \nabla_{\boldsymbol{P}} \boldsymbol{L}\left(\boldsymbol{P}_k, \boldsymbol{\lambda}_{\boldsymbol{G}.k} \right) \tag{28d}$$

$$\boldsymbol{\theta}_k = \begin{cases} 1.0 & \boldsymbol{if} \;\; \boldsymbol{s}_k^T \boldsymbol{J}_k \geq 0.2 \boldsymbol{s}_k^T \boldsymbol{H}_k \boldsymbol{s}_k \\ \dfrac{0.8 \boldsymbol{s}_k^T \boldsymbol{H}_k \boldsymbol{s}_k}{\boldsymbol{s}_k^T \boldsymbol{H}_k \boldsymbol{s}_k - \boldsymbol{s}_k^T \boldsymbol{J}_k} & \boldsymbol{otherwise} \end{cases} \tag{28e}$$

***Step* 6)** Set k=k+1 and start the next iteration from *Step* 2).

Particularly, it is found from (25) that SQP significantly relies on the first-order derivatives which in this paper can be calculated by the eigenvalue sensitivity method [31], as follows:

$$\frac{\partial \lambda_k}{\partial p} = \frac{\partial \lambda_k}{\partial a_{ij}} \frac{\partial a_{ij}}{\partial p} = v_k^T \frac{\partial \boldsymbol{A}}{\partial a_{ij}} u_k \frac{\partial a_{ij}}{\partial p} \tag{29}$$

where λ_k is the kth eigenvalue of matrix $\boldsymbol{A}$ and p is a parameter variable of damping controllers; u_k and v_k are the kth right and left eigenvectors, respectively, of $\boldsymbol{A}$; a_{ij} is the element locating in the ith row, jth column of $\boldsymbol{A}$. Based on (29), the first-order derivatives of the objective and constraints functions for the subproblem (25) can be computed. In this paper, the embedded function *fmincon* in the *Optimization Toolbox*/*Matlab* [32] is used as an effective solver to implement this algorithm with specific supply of the first-order derivatives.

V. Simulations of Proposed Optimal Coordination of PSSs and SDCs

A. New England and New York Interconnected System

A 5-area 16-machine test system (known as New England and New York Interconnected system), as shown in Fig. 6, is used to demonstrate the effectiveness of the proposed control design with multiple inter-area modes. As mentioned in [33], supplementary damping control has been proposed for various controlled plants such as FACTs and HVDC to assist PSS for enhancing the damping of inter-area oscillations in this system. [25]. In this paper, the supplementary damping control implemented in DFIGs will be studied to cooperate with PSSs for controlling weakly damped inter-area modes.

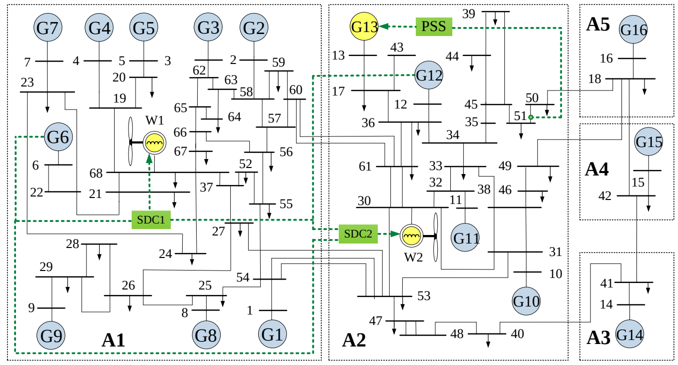

Fig. 6. New England and New York interconnected system with two DFIGs.

Two equivalent DFIG-based WTGs (W1 and W2) are connected at Bus 68 and Bus 30, as shown in Fig. 6, with active power outputs of 745 and 525 MW in the nominal operating condition, respectively. Details on how this equivalence is conducted are introduced in [34]. The parameters of the two DFIGs are same and given in Appendix B. All data in per unit are calculated on the basis of power rating of 100MVA. In this test system, electromechanical oscillations of the local modes have been well damped by local PSSs. However, the system still has two poorly damped inter-area modes: M1 and M2. M1, with the frequency of about 0.37 Hz, dominates the oscillations of generators in A1, A2 with respect to generators in the rest of system. M2 has the frequency of about 0.66 Hz, describing the relative motions between generators in A1 and A2. Thus, a wide-area PSS is installed in G13 to damp the two inter-area modes. Moreover, W1 and W2 are proposed to equip dual-channel SDCs that assist the PSS in achieving the required damping control effects.

According to the residue analysis, a wide-area feedback signal that results in a large residue magnitude with respect to an inter-area mode can be selected as the input signal for the corresponding control loop aiming at this mode [25]. In this test system, the active power of Line 50-51 and the power angle difference between G6 and G12 are selected as two wide-area input signals for the PSS and dual-channel SDCs, respectively. Moreover, the selections also have an additional benefit that the formed control loops have minimal impact on other modes.

By virtue of the Schur method introduced in Subsection III-A, the open-loop power system (with a dimension of 207) is approximately represented by a 43-order model. The model reduction is conducted in a computing platform with Intel Dual-Core i5-4200u CPU of 1.60 GHz and 4.00 GB RAM and takes about 1.65s to finish the computation. The frequency responses of the open-loop system (input-output pairs corresponding to the PSS and the active power channel of SDC in W1) are illustrated in Fig. 7. It is clearly seen that the reduced-order model can be employed to accurately represent the full-order power system within the frequency range concerning the inter-area oscillations (M1 and M2) and even shaft dynamics. Hence, the reduced-order model of the test system is utilized to coordinately design the PSS and SDCs. Particularly, the symbols ‘-P’ and ‘-Q’ in Fig. 7 indicate that the parameters are applied to the PM and QM channels of SDC, respectively (Fig. 4). Moreover, the communication time delays of dedicated signal transmission channels are set to 150 ms [35], and they are approximated by the second-order Pade formula (8).

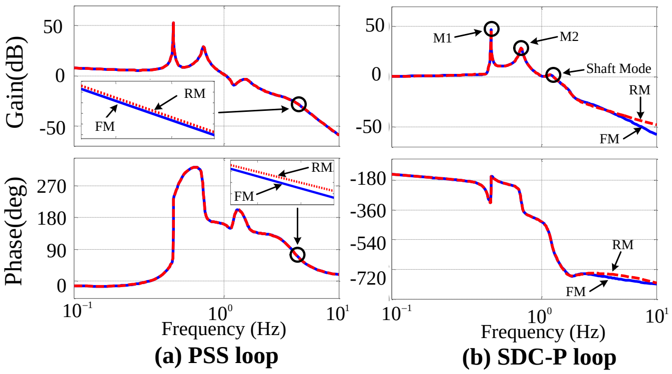

Fig. 7. Open-loop frequency responses for the PSS and the PM-loop of SDC. (solid blue line: the full-order model (FM); dot red line: the reduced-order model (RM))

B. *Effectiveness of Proposed Control Strategy*

To ensure the robustness of designed damping controllers in this test system, six typical operating conditions [25] are selected by changing network configurations, power outputs of two DFIGs and transmitting different levels of power between A1 and A2. The first five operating conditions are used for the design and the last one is used to verify the robustness of designed controllers. The detailed descriptions of these operating conditions are demonstrated in Table I. In particular, the nominal operating condition in this subsection will be employed as a typical example to examine the effectiveness of the proposed control design method in detail.

TABLE I
TYPICAL OPERATING CONDITIONS FOR DESIGN AND VERIFICATION

No.	Description
1	Nominal operating condition
2	One of tie-lines between buses 53-54 is outage
3	One of tie-lines between buses 60-61 is outage
4	One of tie-lines between buses 27-53 is outage
5	Power output of W2 is 100 MW, and active power flow of tie-line 60-61 is 900 MW
6	Power outputs of W1 and W2 are 500 and 300 MW, respectively, and active power flow of tie-line 60-61 is 150 MW

As a comparison, the classic optimization method which mainly focuses on the damping ratios [24] is used to design the PSS and SDC without considering the dynamics of G13 and the two DFIGs; and the obtained controllers are identified as 'SPSS' and 'SSDC' in this paper.

Furthermore, the indexes f_v, f_p, and f_q in the proposed optimization model (21) are normalized to the same order of magnitude to facilitate selection of the weights. Then, the weights of the PSS and two SDCs are chosen to be $\omega_{p1}=\omega_{p2}=1$, $\omega_{q1}=\omega_{q2}=0.8$, and $\omega_v=0.5$ by a trial and error method. Here, the optimal PSS and dual-channel SDCs are obtained after solving the optimization model (21) and labeled by 'OPSS' and 'OSDC'. Moreover, the detailed parameters of the damping controllers are shown in Table V of Appendix C. In addition, to guarantee the final convergence, three feasible initial solutions of the optimization (Case 1, 3, and 5) are tried with SQP and the corresponding iterative processes are depicted in Fig. 16 of Appendix D. Furthermore, the time constant T_w in the washout block is set to be 10 s.

Firstly, the singular values of the cost matrices $\boldsymbol{M}$ in the nominal operating condition are calculated to represent dynamic performance of the SGs and DFIGs, as depicted in Fig. 8 (only the two dominant/largest singular values of each $\boldsymbol{M}$ are plotted). It is obvious that the singular values are decreased when OPSS and OSDC are installed, compared to those in the case with SPSS and SSDC installed. Therefore, it can be preliminarily inferred that G13 and the two DFIGs under the control of OPSS and OSDC would acquire better dynamics during the damping control process.

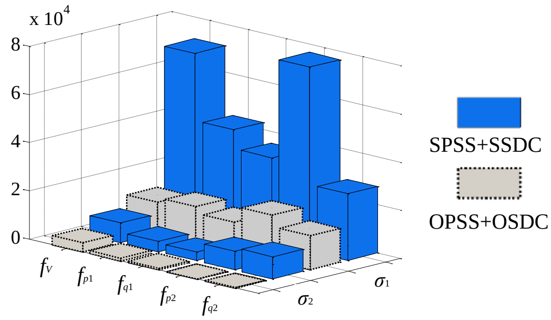

Fig. 8. Singular values of cost matrices $\boldsymbol{M}$ with different controllers.

Next, the eigenvalue analysis is conducted to demonstrate damping effects of the controllers designed by the two methods. Eigenvalues of the closed-loop test system are presented in Table II. M1 and M2 are the inter-area modes and the targets for damping enhancement. Their damping ratios are required to be no less than 20% and 10%, respectively, in this paper. M3 and M4 are also two inter-area modes but with adequate damping already in the open-loop state. M5 and M6 are the shaft modes of the two DFIGs and their damping ratios should be larger than 10 % by the proposed optimization model. In the case of only the PSS working, M1 is with sufficient damping while M2 is still poorly damped. However, when the damping control burden of M2 is appropriately shared by the dual-channel SDCs installed in the DFIGs W1 and W2, these two modes are both satisfactorily controlled. Obviously, it is beneficial to enhance the damping ratios of multiple inter-area modes by dual-channel SDCs. Specifically, the damping of the shaft modes M5 and M6 are weakened by the additionally equipped SDC. Even so, the favorable thing is that OSDC still results in much less extent of such damping deterioration than SSDC.

Furthermore, time domain simulations are conducted to confirm the above analysis. An instantaneous three-phase short circuit fault occurs at Bus 60 in A1 at 1.0 s and it is self-cleared 100 ms later [33]. The relative power angles of G15 vs. G13 and G6 vs. G13 can be used to clearly observe the modes of M1 and M2, respectively, as shown in Fig. 9. When only the PSS is installed in G13, the dynamics associated with M2 are mildly affected. But, the dual-channel SDCs can supplementally provide required damping to M1 and M2 simultaneously (the power angle oscillation related to M2 is suppressed within 10 s). However, the main distinctions between the controllers designed by the conventional method and the proposed method are the resulted dynamics of G13 and the DFIGs during the transient period, as shown in Figs. 10 and 11. Because the proposed method can optimize the dynamics of G13 and DFIGs by reducing the indexes f_v, f_p, and f_q, the test system controlled by OPSS and OSDC has the least fluctuant dynamics in the terminal voltage of G13 (Fig. 10). Moreover, Figs. 11 and 12 show that the dynamics of two DFIGs' power outputs are also improved when OPSS and OSDC are employed. SPSS and SSDC can also effectively suppress inter-area oscillations but with obviously adverse impacts on the dynamics of the DFIGs. This is because the exclusive objective of the classic method is to damp inter-area oscillations. In particular, the shaft modes of the two DFIGs are observed in the dynamics of their turbine speeds ω_t in Fig. 12. It is seen that the torsional oscillations with OSDC have pretty satisfactory damping in contrast to the weakly damped oscillations with SSDC installed. Therefore, it is clearly verified by the above simulations that the proposed method can not only well damp inter-area oscillations by coordinating the PSS and SDC but also guarantee the optimal dynamics of controlled plants.

TABLE II
RESULTS OF EIGENVALUE ANALYSIS

Mode	No controller	Only PSS	SPSS and SSDC	OPSS and OSDC
M1	0.002±2.29i (ξ=-0.1%)	-0.402±2.13i (ξ=18.5%)	-0.525±2.02i (ξ=25.1%)	-0.655±2.29i (ξ=27.9%)
M2	-0.102±4.17i (ξ=2.4%)	-0.217±4.17i (ξ=5.2%)	-0.494±4.42i (ξ=11.1%)	-0.616±4.23i (ξ=14.4%)
M3	-0.589±2.94i (ξ=19.6%)	-0.571±2.93i (ξ=19.1%)	-0.564±2.93i (ξ=18.9%)	-0.593±2.93i (ξ=19.8%)
M4	-0.791±4.57i (ξ=17.1%)	-0.799±4.54i (ξ=17.3%)	-0.779±4.49i (ξ=17.1%)	-0.817±4.58i (ξ=17.6%)
M5	-0.826±7.44i (ξ=11.0%)	-0.826±7.44i (ξ=11.0%)	-0.425±7.53i (ξ=5.6%)	-0.762±7.51i (ξ=10.1%)
M6	-0.833±7.48i (ξ=11.1%)	-0.733±7.48i (ξ=9.8%)	-0.448±7.39i (ξ=6.1%)	-0.744±7.39i (ξ=10.0%)

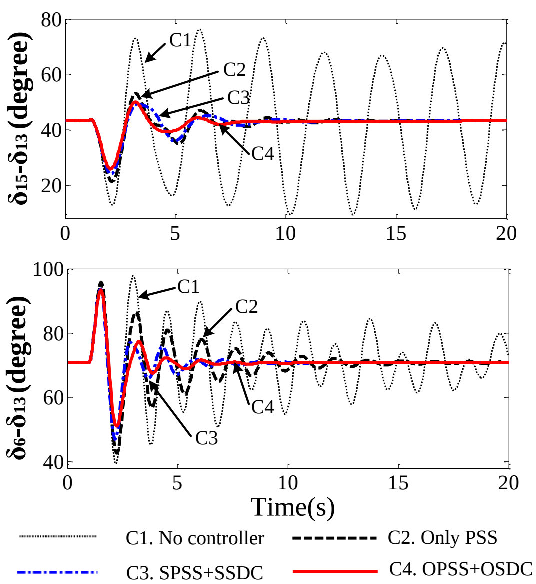

Fig. 9. Dynamics of relative power angles.

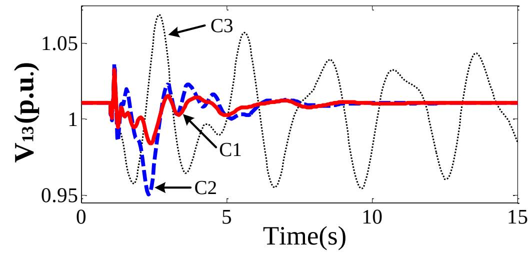

Fig. 10. Dynamics of terminal voltage of G13 (solid line- C1: OPSS+OSDC; dotted line– C2: SPSS+SSDC; dashed line- C3: no controller).

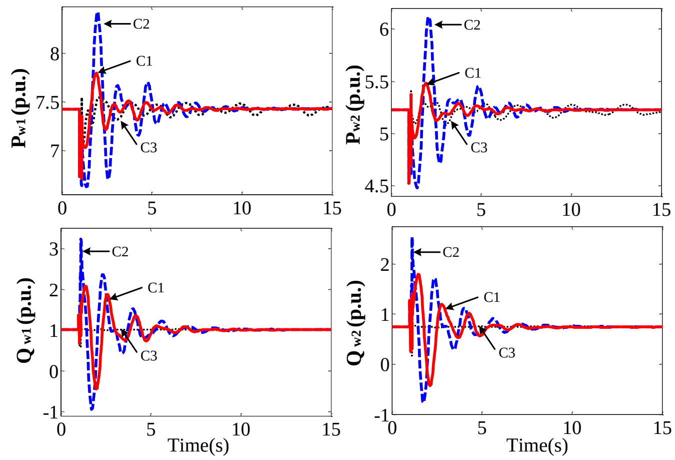

Fig. 11. Dynamics associated with two DFIGs (solid line- C1: OPSS+OSDC; dotted line- C2: SPSS+SSDC; dashed line- C3: no controller).

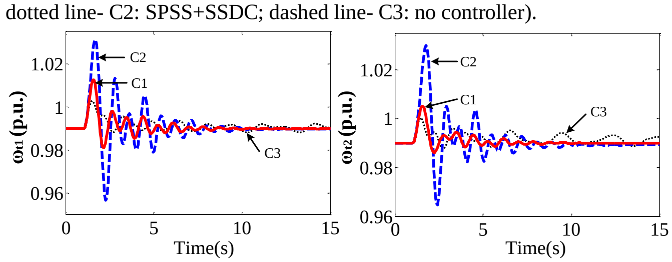

Fig. 12. Torsional dynamics of two DFIGs (solid line- C1: OPSS+OSDC; dot ted line- C2: SPSS+SSDC; dashed line- C3: no controller).

C. Verification of Robustness of Proposed Control Design

In the previous subsection, the effectiveness of proposed control design has been verified at the nominal operating condition. Moreover, the robust performance of proposed control design in other different operating conditions (Table I), especially the operating conditions with tie-line outages, is validated in this subsection. The modal analysis of this test system is carried out for these operating conditions when the two methods are respectively used for designing the damping controllers of the closed-loop system (Table III). Because the robustness has been considered in the two methods by directly using the first five operating conditions for formation of the objective function, it is not surprised that the damping ratios of the inter-area modes M1 and M2 are finally acceptable and better than those in the open-loop states. Nevertheless, the main advantage of proposed control design method is to simultaneously optimize the dynamic performance of controlled plants.

Time domain simulations over all the operating conditions are further conducted to verify the robust optimization of controlled plants' dynamics by the proposed design method. Dynamics of two deviation variables of W1 (ΔP_{w1} and ΔQ_{w1}) are depicted in Fig. 13. It can be found that the curves of ΔP_{w1} and

ΔQ_{w1} with OSDC have less fluctuation than the curves with SSDC in all the operating conditions. Moreover, envelops of the curves clusters are also added in Fig. 13. The darkly colored area under the envelop corresponding to OSDC is much smaller than the lightly colored area associated with SSDC. All these comparisons prove that the OSDC performs better than the SSDC in very wide operating conditions. In particular, due to the poorly damped shaft mode, the DFIG controlled by SSDC has comparatively more fluctuant dynamics in the rear section of the curve of ΔP_{w1}.

TABLE III
DAMPING RATIOS OF TWO INTER-AREA MODES FOR DIFFERENT OPERATING CONDITIONS

No.	Mode	No controller	SPSS and SSDC	OPSS and OSDC
2	M1	-0.024±2.241i (ξ=1.1%)	-0.464±1.996i (ξ=22.6%)	-0.585±2.080i (ξ=27.1%)
	M2	-0.081±3.966i (ξ=2.0%)	-0.574±4.245i (ξ=13.4%)	-0.654±4.076i (ξ=15.8%)
3	M1	0.017±2.267i (ξ=0.7%)	-0.468±2.019i (ξ=22.6%)	-0.592±2.057i (ξ=27.7%)
	M2	-0.079±3.964i (ξ=2.0%)	-0.567±4.251i (ξ=13.2%)	-0.650±4.060i (ξ=15.8%)
4	M1	0.004±2.270i (ξ=-0.2%)	-0.472±2.021i (ξ=22.7%)	-0.571±2.035i (ξ=27.0%)
	M2	-0.099+4.123i (ξ=2.4%)	-0.587±4.427i (ξ=13.1%)	-0.625±4.191i (ξ=14.7%)
5	M1	0.081±2.217i (ξ=-3.7%)	-0.427+2.003i (ξ=20.8%)	-0.516±2.230i (ξ=22.5%)
	M2	-0.165±3.650i (ξ=4.5%)	-0.689±4.046i (ξ=16.8%)	-0.718±3.788i (ξ=18.6%)
6	M1	0.0243±2.029i (ξ=-1.2%)	-0.510±2.017i (ξ=24.5%)	-0.646±2.039i (ξ=30.2%)
	M2	-0.069±4.346i (ξ=1.6%)	-0.581±4.652i (ξ=12.4%)	-0.636±4.424i (ξ=14.2%)

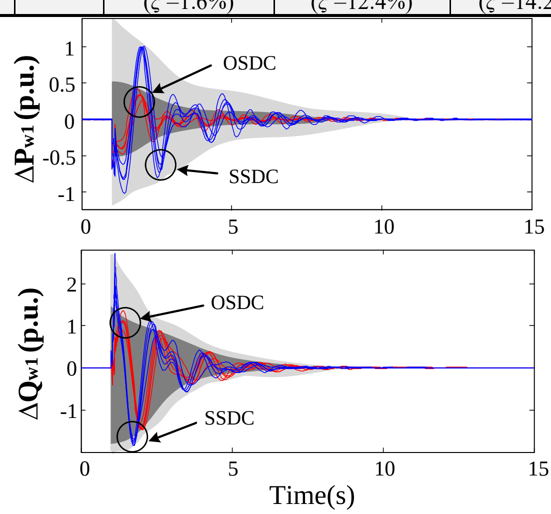

Fig. 13. Power outputs of W1. (red line: OSDC; blue line: SSDC)

D. Effects of the Optimization Weights on the Control Results

As one meaningful contribution of this paper, the proposed control design can reasonably and flexibly allocate the damping control burden between the PSS and dual-channel SDC. In the meantime, as discussed in Subsection IV-B, the smaller weight in (21) will lead to more obvious dynamics fluctuations of the corresponding controlled plant. Therefore, to further validate this conclusion, three typical sets of weights are employed for the optimization model (21), as shown in Table IV.

TABLE IV
THREE SETS OF WEIGHTS FOR OPTIMIZATION MODEL

Set No.	ω_v	ω_{p1}	ω_{q1}	ω_{p2}	ω_{q2}
1	1	0.5	0.8	0.5	0.8
2	0.7	1	0.3	1	0.3
3	0.2	1	0.8	1	0.8

Due to the constraints (21b) associated with damping ratios of the two inter-area modes, the consequent damping effects with different weights are slightly distinct while the dynamic performance of controlled plants is clearly different. Correspondingly, the comparative results by the time domain simulations are illustrated in Figs. 14 and 15. It can be seen in Fig. 14 that because the weight ω_p in Set 1 is the smallest, the resulted dynamical curves of active power outputs of W1 and W2 are more fluctuant than their opponents. Similarly, as for Set 2, the dynamics relevant to reactive power outputs of W1 and W2 are apparently deteriorated due to the lowest weights for exhaustive use of the QM channel. Finally, since the weights in Set 3 make G13 sharing the most damping control burden, the fluctuation of its terminal voltage is the most obvious, as shown in Fig. 15.

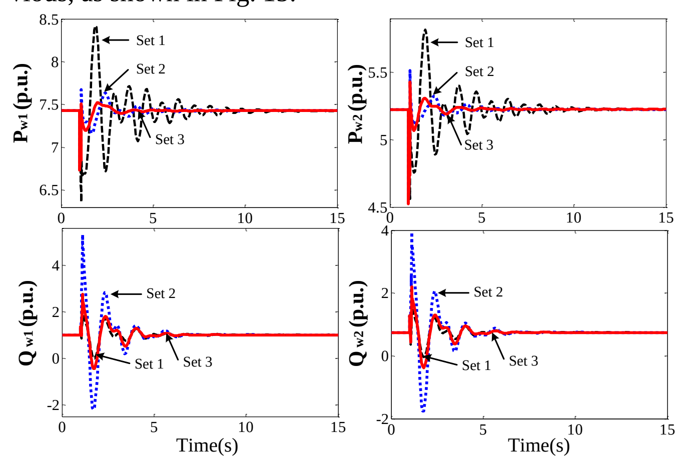

Fig. 14. Output power dynamics of two DFIGs with three sets of weights (dashed line: Set 1; dotted line: Set 2; solid line: Set 3).

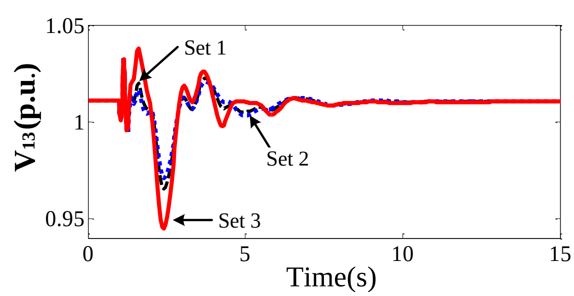

Fig. 15. Terminal voltage of G13 with three sets of weights (dashed line: Set 1; dotted line: Set 2; solid line: Set 3).

VI. CONCLUSION

Modulation of DFIG by a dual-channel SDC is utilized in this paper to cooperate with the PSS for damping inter-area oscillations. It is known that the dynamics of the DFIG (e.g. the shaft mode) could be obviously deteriorated if the SDC is inappropriately tuned. Therefore, by using a performance index to quantitatively gauge the controlled plants' dynamics, the optimization based design method can not only meet the required damping effects on inter-area oscillations but also optimize the dynamics of the SG and DFIG. Furthermore, the proposed method is able to reasonably and flexibly assign the damping control burden among the SDC and PSS.

Application of the proposed design method on the modified New England and New York interconnected system validates that the inter-area modes are sufficiently damped by the coordinated PSS and SDC across different operating conditions. Moreover, the SG and DFIG have optimal dynamics as they are driven to participate in the damping control. For example, the shaft dynamics remain acceptable even when the DFIG contributes to the damping control with the well-tuned SDC. In addition, effects of the weights in the optimization model are also discussed and verified.

APPENDIX

A. Linearized Model of the Closed-Loop Power System

For an open-loop power system, its linearized model on the jth operating condition can be further approximated through a reduced-order model based on the Schur method introduced in Subsection III-A. Moreover, the models of wide-area communication time delays and damping controllers (PSSs and SDCs) can also be expressed by the form of state space equations. These models are presented in the following and they can be readily synthesized to derive the linearized state-space model of the closed-loop power system.

$$\begin{cases} \dot{\boldsymbol{x}}_{jr} = \boldsymbol{A}_{jr}\boldsymbol{x}_{jr} + \boldsymbol{B}_{jr}\boldsymbol{u}_c \\ \boldsymbol{y}_{jo} = \boldsymbol{C}_{jc}\boldsymbol{x}_{jr} \end{cases} \tag{30}$$

$$\begin{cases} \dot{\boldsymbol{x}}_{\tau} = \boldsymbol{A}_{\tau}\boldsymbol{x}_{\tau} + \boldsymbol{B}_{\tau}\boldsymbol{y}_{jo} \\ \boldsymbol{y}_{d} = \boldsymbol{C}_{\tau}\boldsymbol{x}_{\tau} + \boldsymbol{D}_{\tau}\boldsymbol{y}_{jo} \end{cases} \tag{31}$$

$$\begin{cases} \dot{\boldsymbol{x}}_{c} = \boldsymbol{A}_{c}\boldsymbol{x}_{c} + \boldsymbol{B}_{c}\boldsymbol{y}_{d} \\ \boldsymbol{u}_{c} = \boldsymbol{C}_{c}\boldsymbol{x}_{c} + \boldsymbol{D}_{c}\boldsymbol{y}_{d} \end{cases} \tag{32}$$

where $\boldsymbol{x}_{jr}$, $\boldsymbol{x}_{\tau}$, and $\boldsymbol{x}_c$ are the state variables vectors, respectively, of the reduced-order open-loop power system, the approximated time-delays and the damping controllers; $\boldsymbol{u}_c$ is the output vector of the damping controllers and also the input vector of the open-loop system; $\boldsymbol{y}_d$ represents the delayed output of the system's observation $\boldsymbol{y}_{jo}$. Overall, the matrix of the closed-loop power system in (9) can be obtained, as follows:

$$\boldsymbol{x}_j = \left[\boldsymbol{x}_{jr}\ \boldsymbol{x}_{\tau}\ \boldsymbol{x}_c\right]^{\boldsymbol{T}} \quad \boldsymbol{E}_j = \left[\boldsymbol{C}_{jr}\ \boldsymbol{0}\ \boldsymbol{0}\right] \quad \boldsymbol{K}_j = \left[\boldsymbol{0}\ \boldsymbol{0}\ \boldsymbol{C}_c\right] \tag{33}$$

B. Parameters of the DFIG

DFIG Parameters on Base of Machine Ratings, 900 MVA and 20 kV: R_s = 0.0049 p.u.; R_r = 0.0055 p.u.; L_s = 0.0924 p.u.; L_r = 0.0996 p.u.; L_m = 3.953 p.u.; H_g =1.2 s; X_{tg} = 0.0055 p.u.; H_t = 3.8 s; K_{tw} = 0.4 (p.u./rad); D_{tw} = 0.025 p.u..

C. Parameters of Damping Controllers

TABLE V
PARAMETERS OF PSS AND DUAL-CHANNEL SDC

	K/p.u.	T_1/s	T_2/s	T_3/s	T_4/s
Conventional optimization					
SPSS	0.0021	1.4629	0.1661	1.5629	0.1261
SSDC-P1	0.9500	0.6572	0.1408	0.6572	0.1510
SSDC-Q1	0.6330	0.7031	0.1836	0.7126	0.1837
SSDC-P2	1.6835	0.5568	0.2327	0.5568	0.2378
SSDC-Q2	0.9632	0.8510	0.4134	0.8510	0.4134
Proposed optimization					
OPSS	0.0049	1.1657	0.2716	1.0742	0.2357
OSDC-P1	0.2156	0.9317	0.0598	0.8211	0.0485
OSDC-Q1	0.2490	1.2193	0.0462	1.3190	0.0652
OSDC-P2	0.1817	0.6871	0.0867	0.7281	0.1057
OSDC-Q2	0.2267	1.0706	0.0566	1.0701	0.0549

D. Searching Process of SQP

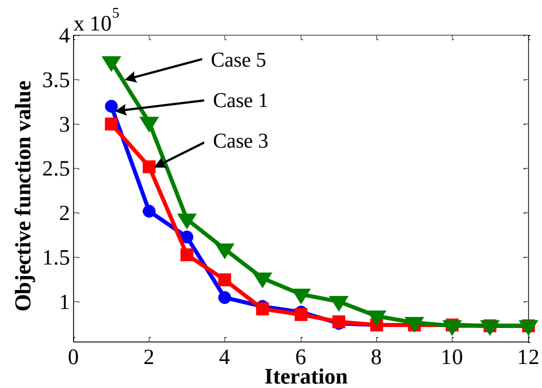

Fig. 16. Searching process of SQP with different initial solutions. (●: Case 1; ■: Case 3; ▲: Case 5)

REFERENCES

[1] L. P. Kunjumuhammed, B. C. Pal, C. Oates, and K. J. Dyke, "Electrical oscillations in wind farm systems: analysis and insight based on detailed modeling," *IEEE Trans. Sustain. Energy*, vol. 7, no. 1, pp. 51-62, Jan. 2016.

[2] J. Hu, Y. Huang, D. Wang, H. Yuan, and X. Yuan, "Modeling of grid-connected DFIG-based wind turbines for DC-link voltage stability analysis," *IEEE Trans. Sustain. Energy*, vol. 6, no. 4, pp. 1325-1336, Oct. 2015.

[3] M. Edrah, K. L. Lo, and O. Anaya-Lara, "Impacts of high penetration of DFIG wind turbines on rotor angle stability of power systems," *IEEE Trans. Sustain. Energy*, vol. 6, no. 3, pp. 759-766, Jul. 2015.

[4] D. Gautam, V. Vittal, and T. Harbour, "Impact of increased penetration of DFIG-based wind turbine generators on transient and small signal stability of power systems," *IEEE Trans. Power Syst.*, vol. 24, no. 3, pp. 1426-1434, Aug. 2009.

[5] W. Du, J. Bi, J. Cao and H. F. Wang, "A method to examine the impact of grid connection of the DFIGs on power system electromechanical oscillation modes," *IEEE Trans. Power Syst.*, vol. 31, no. 5, pp. 3775-3784, Sep. 2016.

[6] J. Morato, T. Knuppel, and J. Ostergaard, "Residue-based evaluation of the use of wind power plants with full converter wind turbines for power oscillation damping control," *IEEE Trans. Sustain. Energy*, vol. 5, no. 1, pp. 82-89, Jan. 2014.

[7] J. L. Dominguez-Carcia, O. Gomis-Bellmunt, F. D. Bianchi, and A. Sumper, "Power oscillation damping supported by wind power: A review," *Renew. Sustain. Energy Rev.*, vol. 16, no. 7, pp. 4982-4993, Sep. 2012.

[8] H. A. Mohammadpour, and E. Santi, "SSR damping controller design and optimal placement in rotor-side and grid-side converters of series-compensated DFIG-based wind farm," *IEEE Trans. Sustain. Energy*, vol. 6, no. 2, pp. 388-399, Apr. 2015.

[9] F. M. Hughes, O. Anaya-Lara, N. Jenkins, and G. Strbac, "A power system stabilizer for DFIG-based wind generation," *IEEE Trans. Power Syst.*, vol. 21, no. 2, pp. 763-772, May. 2006.

[10] Z. Miao, L. Fan, D. Osborn, S. Yuvarajan, "Control of DFIG-based wind generation to improve inter-area oscillation damping," *IEEE Trans. Energy Convers.*, vol. 24, no. 2, pp. 415-422, Jun. 2009.
[11] Y. Mishra, S. Mishra, M. Tripathy, N. Senroy, and Z. Y. Dong, "Improving stability of a DFIG-based wind power system with tuned damping controller," *IEEE Trans. Energy Convers.*, vol. 24, no. 3, pp. 650-660, Sep. 2009.
[12] Y. Wang, J. Meng, X. Zhang, and L. Xu, "Control of PMSG-based wind turbines for system inertial response and power oscillation damping," *IEEE Trans. Sustain. Energy*, vol. 6, no. 2, pp. 565-574, Apr. 2015.
[13] Y. Liu, J. R. Gracia, T. J. King, and Y. Liu, "Frequency regulation and oscillation damping contributions of variable-speed wind generators in the U.S. Eastern Interconnection (EI)," *IEEE Trans. Sustain. Energy*, vol. 6, no. 3, pp. 951-957, Jul. 2015.
[14] M. Singh, A. J. Allen, E. Muljadi, V. Gevorgian, Y. Zhang, and S. Santoso, "Interarea oscillation damping controls for wind power plants," *IEEE Trans. Sustain. Energy*, vol. 6, no. 3, pp. 967-975, Jul. 2015.
[15] H. Yin, L. Fan, and Z. Miao, "Reactive power modulation for inter-area oscillation damping of DFIG-based wind generation," in *Proc. IEEE Power Energy Soc. Gen. Meeting*, Minneapolis, US, 2010, pp. 1-9.
[16] K. Liao, Z. He, Y. Xu, G. Chen, Z. Y. Dong, and K. P. Wang, "A sliding mode based damping control of DFIG for interarea power oscillations," *IEEE Trans. Sustain. Energy*, vol. 8, no. 1, pp. 258-267, Jan. 2017.
[17] M. Mokhtari, F. Aminifar, "Toward wide-area oscillation control through doubly-fed induction generator wind farms," *IEEE Trans. Power Syst.*, vol. 29, no. 6, pp. 2985-2992, Nov. 2014.
[18] E. Vittal, M. O'Malley, A. Keane, "Rotor angle stability with high penetrations of wind generation," *IEEE Trans. Power Syst.*, vol. 27, no. 1, pp. 353-362, Feb. 2012.
[19] L. Fan, H. Yin, and Z. Miao, "On active/reactive power modulation of DFIG-based wind generation for inter-area oscillation damping," *IEEE Trans. Energy Convers.*, vol. 26, no. 2, pp. 513-521, Jun. 2011.
[20] N. Kshatriya, U. D. Annakkage, F. M. Hughes, and A.M. Gole, "Optimized partial eigenstructure assignment-based design of a combined PSS and active damping controller for a DFIG," *IEEE Trans. Power Syst.*, vol. 25, no. 2, pp. 866-876, May. 2010.
[21] T. Surinkaew, I. Ngamroo, "Hierarchical co-ordinated wide area and local controls of DFIG wind turbine and PSS for robust power oscillation damping," *IEEE Trans. Sustain. Energy*, vol. 7, no. 3, pp. 943-955, Jul. 2016.
[22] H. Huang, C. Y. Chung, "Coordinated damping control design for DFIG-based wind generation considering power output variation," *IEEE Trans. Power Syst.*, vol. 27, no. 4, pp. 1916-1925, Nov. 2012.
[23] S. M. Barakati, M. Kazerani, and J. D. Aplevich, "Maximum power tracking control for a wind turbine system including a matrix converter," *IEEE Trans. Energy Convers.*, vol. 24, no. 3, pp. 705-713, Sep. 2009.
[24] N. R. Chaudhuri, and B. Chaudhuri, "Considerations toward coordinated control of DFIG-based wind farms," *IEEE Trans. Power Del.*, vol. 28, no. 3, pp. 1263–1270, Jul. 2013.
[25] B. Pal and B. Chaudhuri, *Robust Control in Power Systems*, New York: Springer, 2005.
[26] S. Ghosh, K. A. Folly, and A. Patel, "Synchronized versus non-synchronized feedback for speed-based wide-area PSS: effect of time-delay," *IEEE Trans. Smart Grid*, early access.
[27] D. P. Ke, C. Y. Chung, Y. Xue, "An eigenstructure-based performance index and its application to control design for damping inter-area oscillations in power systems," *IEEE Trans. Power Syst.*, vol. 26, no. 4, pp. 2371-2380, Nov. 2011.
[28] G. J. W. Dudgeon, W. E. Leithead, A. Dysko, J. OReilly, and J. R. McDonald, "The effective role of AVR and PSS in power systems: frequency response analysis," *IEEE Trans. Power Syst.*, vol. 22, no. 4, pp. 1986-1994, Nov. 2007.
[29] J. Zhang, C. Y. Chung, C. Lu, K Men, and L. Tu, "A novel adaptive wide area PSS based on output-only modal analysis," *IEEE Trans. Power Syst.*, vol. 30, no. 5, pp. 2633-2642, Sep. 2015.
[30] J. Nocedal and S. J. Wright, *Numerical Optimization*. New York: Springer, 2006.
[31] F. L. Pagola, I. J. Perez-Arriaga, and G. C. Verghese, "On sensitivities, residues and participations: applications to oscillatory stability analysis and control," *IEEE Trans. Power Syst.*, vol. 4, no. 1, pp. 278-285, Feb. 1989.
[32] "*Matlab User's Guide*," MathWorks, Natick, MA, 2013.
[33] C. Canizares, T. Fernandes, E. Geraldi, *et al*., "Benchmark models for the analysis and control of small-signal oscillatory dynamics in power systems," *IEEE Trans. Power Syst.*, vol. 32, no. 1, pp. 715-722, Jan. 2017.
[34] E. Muljadi, C. P. Butterfield, A. Ellis, *et al*., "Equivalencing the collector system of a large wind power plant," in *Proc. IEEE Power Eng. Soc. Gen. Meeting*, Montreal, Canada, 2006, pp. 1-8.
[35] M. Beiraghi and A. M. Ranjbar, "Adaptive delay compensator for the robust wide-area damping controller design," *IEEE Trans. Power Syst.*, vol. 31, no. 6, pp. 4966-4976, Nov. 2016.

Chen Zhang (S'16) received the B.S degree in Electrical Engineering in 2014 from Wuhan University, Wuhan, China. Currently, he is pursuing the Ph.D. degree in the School of Electrical Engineering, Wuhan University. At present, he is also funded by Chinese Scholarship Council (CSC) as a joint Ph.D. student in the Department of Electrical Engineering and Computer Science, Case Western Reserve University, Cleveland, Ohio, USA.

His research interests are in power system stability and control, wind power, and direct load control.

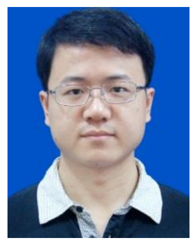

Deping Ke received the B.S degree in Electrical Engineering in 2005 from Huazhong University of Science and Technology, Wuhan, China, and the Ph.D. degree in Electrical Engineering from The Hong Kong Polytechnic University in 2012. Currently, he is an Associate Professor with the School of Electrical Engineering, Wuhan University, China.

His research interests are in power system dynamics and control, and economic operation of power systems.

Yuanzhang Sun (M'99-SM'01) received the B.S. degree from Wuhan University of Hydro and Electrical Engineering, Wuhan, China, in 1987, the M.S. degree from the Electric Power Research Institute(EPRI), Beijing, China, in 1982, and the Ph.D. degree in electrical engineering from Tsinghua University, Beijing, in 1988.

Currently, he is a Professor of the School of Electrical Engineering at Wuhan University, and a Chair Professor of the Department of Electrical Engineering and Vice Director of the State Key Lab of Power System Control and Simulation at Tsinghua University. His main research interests are in the areas of power system dynamics and control, wind power, voltage stability and control, and reliability.

C. Y. Chung (M'01–SM'07–F'16) received the Ph.D. degree in electrical engineering from The Hong Kong Polytechnic University in 1999. He is currently a Professor and the SaskPower Chair in Power Systems Engineering in the Department of Electrical and Computer Engineering at the University of Saskatchewan, Saskatoon, SK, Canada.

His research interests include power system stability/control, planning and operation, computational intelligence applications, power markets, and electric vehicle charging.

Dr. Chung is an Editor of the IEEE TRANSACTIONS ON SUSTAINABLE ENERGY and the IEEE TRANSACTIONS ON POWER SYSTEMS. He is also an Editorial Board Member of IET GENERATION, TRANSMISSION & DISTRIBUTION. He is also a Member-at-Large (Smart Grid) of IEEE PES Governing Board and the IEEE PES Region 10 North Chapter Representative.

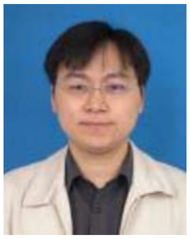

Jian Xu (M'08) received the Ph.D. degree in electrical engineering from the Wuhan in 2007. He joined Wuhan University as a Lecturer in 2007. Since 2015, he has been a Professor of the School of Electrical Engineering at Wuhan University. During 2013–2014, he was a visiting scholar at the Energy Systems Innovation Center, Washington State University, Pullman, WA, USA.

His research interests include power system stability and control.

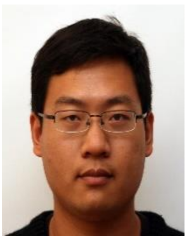

Feifan Shen received the B.S in Electrical Engineering from Hohai University in 2015 and the M.S. in Electrical Engineering from Wuhan University in 2017, respectively. Currently, he is pursuing his PH.D degree in department of electrical engineering at Technical University of Denmark. His research interests include power system stability and control and active distribution networks.